



Journal of Applied and Computational Mechanics



Research Paper

Stress Control of a Piezoelectric Lumped-element Model – Theoretical Investigation and Experimental Realization*

Juergen Schoeftner¹, Andreas Brandl², Hans Irschik³

¹ Institute of Technical Mechanics, Johannes Kepler University Linz, Altenberger Strasse 69, 4040 Linz, Austria, Email: juergen.schoeftner@jku.at

² Institute of Technical Mechanics, Johannes Kepler University Linz, Altenberger Strasse 69, 4040 Linz, Austria, Email: andreas.brandl@jku.at

³ Institute of Technical Mechanics, Johannes Kepler University Linz, Altenberger Strasse 69, 4040 Linz, Austria, Email: hans.irschik@jku.at

* Dedicated to Prof. Casciati and Prof. Faravelli on the occasion of their 70th birthdays.

Received April 20 2020; Revised August 26 2020; Accepted for publication August 27 2020.

Corresponding author: Juergen Schoeftner (juergen.schoeftner@jku.at)

© 2020 Published by Shahid Chamran University of Ahvaz

Abstract. This contribution focuses on force- and stress-tracking of a multi-degree of freedom system by eigenstrain actuation. The example under consideration is an axially excited piezoelectric bar which can be modeled as a lumped parameter system. The piezoelectric effect serves as actuation source and the question is answered how to prescribe the piezoelectric actuation in order to achieve a desired stress distribution, or, in the lumped case, a desired distribution of internal forces. First, the equations of motion are set up in matrix notation where the state vector contains the displacement components. After some basic manipulations, the governing equation can be written in terms of the internal force vector. Now, if one intends to have a certain desired internal force distribution, it is straightforward to find a condition for the piezoelectric control actuation. The developed theory is first verified by using a continuous piezoelectric bar, where the motion of one end is prescribed. Then the theory is experimentally verified: a lumped two-degree of freedom system is investigated and the goal is to reduce the stress or the internal force in order to avoid mechanical damage. The force-controlled configuration is exposed to a sweep-signal excitation between 1000–4900 Hz, running for 22 minutes without any signs of damage. Then the same system is excited by the same excitation but without piezoelectric control. After some seconds the test sample is visibly damaged, going along with a significant reduction of the first eigenfrequency. This gives strong evidence for the appropriateness of the proposed stress or force control methodology.

Keywords: Piezoelectric control, Stress control, Structural control, Fatigue and damage, Lumped parameter system.

1. Introduction

Multi-functional materials are materials that are equipped with smart devices. These smart or intelligent structures take advantage of physical effects, which combine two or more different physical fields. One example is the piezoelectric effect that enables multi-field coupling of mechanical and electrical domain, either for actuation or for sensing, see e.g. [1] – [4]. In this context, on the one hand, sensing means to monitor the motion of a structure (i.e. structural health monitoring). On the other hand, actuation often means displacement tracking where the question is posed how to actuate and to place the piezoelectric materials onto an elastic structure in order to achieve a desired displacement field at one or several locations.

In the present contribution the focus is laid on stress control, which is a rather new research topic, by means of exploiting the piezoelectric effect. Similar to displacement tracking or shape control techniques, the goal of stress control is to lower the stress or the internal force. Both techniques, displacement and stress tracking, are open-loop control methods, hence the system parameters (i.e. geometry, material, external forces) must be known in advance. For literature overviews on shape control and displacement tracking, the reader is referred to [5] – [7]. In [8] dynamic shape control is performed for a hyperelastic solid: the analytical solution is compared to the Finite Element computation for an irregularly shaped object. In [9] adaptive wings with linear displacement actuators inside the wing are controlled such that the cost function containing the drag coefficient and the surface pressure is minimized. A cost function is minimized in [10] in order to compute the best locations for the piezoelectric control plates mounted onto the surface of a cantilever. For harmonic vibrations passive shape control of beam structures is possible with properly shaped piezoelectric layers and electric circuits without any actuation source, see [11] and [12]. The use of moderately conductive electrodes in combination with electric circuits allows for an optimal tuning of the control voltage at desired locations with only one prescribed voltage source, see [13], [14] and [15]. Finally, some other fields (without claim to completeness) are mentioned where piezoelectricity plays an important role: multi-mode control ([29], [30]), acoustic problems ([31]), shunt damping by means of the shear mode ([32], [33]) and damping with moderately conductive electrodes ([34]).



A rather new research topic, stress control of structures via the piezoelectric effect, is the main objective in this contribution. In contrast to displacement tracking, scientific contributions for stress tracking are rare, although stress is known to be the main factor for failure and breakdown of structures: high-cycle fatigue is the failure mode when the stress limit is exceeded for a high number stress cycles, see [16], [17] and [18]. The basis for stress tracking was originated by Irschik [19] and co-workers, see also e.g. [20] and [21], who provided a theoretical three-dimensional framework for stress and displacement control at a continuum mechanics level. In extension, Schoeftner derived new results for structural models, in particular for a bar and for a beam: in [22] the axial stress caused by longitudinal vibrations was investigated and a numerical example is presented how to achieve a desired axial stress distribution generated by several types of support excitations. The frequency spectrum of the excitation was varied and the results showed that low-frequency stress can be reduced, but lower bounds for the stress exist for high-frequency components. Within the Bernoulli-Euler beam framework, bending vibrations of a piezoelectric beam were investigated: the maximal stress usually occurs at the upper or at the lower surface (but not necessarily for piezoelectric structures due to the eigenstrain distribution over the thickness) and it was demonstrated that the axial stress as well as the bending moment can be reduced by proper piezoelectric actuation, see [23]. Based on the outcomes of the above cited theoretical findings and numerical benchmark examples, a simple laboratory experiment was designed in [24] to reduce the stress of a harmonically excited piezoelectric transducer with attached mass. Although several uncertainties of the system parameters are present (e.g. stiffness, piezoelectric constants, masses), it could be demonstrated for a mono-frequent excitation that the controlled configuration remains undamaged, while the uncontrolled configuration suffers severe visible mechanical damage accompanied by a strongly reduced first eigenfrequency. To show this, the frequency response functions were measured before and after the stress-controlled test run (30min). Finally, after the uncontrolled run (that only took some seconds until severe damage) the measured frequency response function showed significant changes to the previous ones.

In the present contribution we derive a matrix-based formulation of stress control: the system under consideration is a lumped-element discretization of a piezoelectric bar. Knowing the matrix differential equations from Newton's law, using the constitutive relations and prescribing the desired temporal and spatial distribution of the internal force vector, one may derive a relation for (the second time-derivative of) the required piezoelectric actuation. The remaining two integration constants follow from the initial state vector, the initial external forces and the initial desired stress distribution. The stress-control solution depends on system parameters (mass, damping, stiffness matrices, piezoelectric constants) and external sources (force- or supported excitation). First, a numerical benchmark example proves our theory. The latter allows for an easy implementation in numerical programs if the mathematical model is known (see also the example in [22], where stress-control of a piezoelectric unimorph was considered as a spatially-distributed parameter system. Moreover, the matrix-based solution for stress control also considers linear damping. In the final experimental part of the present contribution, we demonstrate a strong reduction of the longitudinal stress in a piezoelectric control device, which is excited by a chirp signal (frequency content between 1000–4900 Hz). After measuring the original frequency response function (FRF between the actuator signal and the velocity signal of the mass), the repeating chirp disturbance and proposed piezoelectric stress-control actuation do not cause any damage of the experimental setup. At the end of this test run, practically the same low-excitation FRF could be measured again, which gave evidence for an undamaged configuration. Afterwards, the setup was excited by the same excitation but without stress-control actuation. After a comparatively low number of cycles, the internal force/stress exceeded the stress limit, causing an irreparable damage of the piezoelectric transducer. The structural damage went along with a significant reduction of the first resonance frequency, providing strong evidence for the appropriateness of the proposed stress or force control methodology.

2. Modeling and Stress-control of a Piezoelectric Bar

In this section, we first derive the conditions for the stress- or force control of a multi-degree of freedom system that consists of discrete masses, springs and actuation forces. Fig.1 depicts a piezoelectric bar with electrodes at the upper and lower surfaces. This system is split into single masses between which the internal forces (spring, damping and actuation forces) act (Fig.1b). We first explicitly write down the equations of motion for the three-degree-of-freedom model for didactical reasons. These equations can be generalized in such a manner that they hold for a general system with n degrees of freedom (DOF), which is written in matrix notation.

Applying Newton's law for the three masses one finds

$$\begin{aligned}
 m\ddot{u}_1 &= -F_{01} + F_{12} + F_{\text{ext}F1} \\
 m\ddot{u}_2 &= -F_{12} + F_{23} + F_{\text{ext}F2} \\
 m\ddot{u}_3 &= -F_{23} + F_{\text{ext}F3}
 \end{aligned}
 \rightarrow
 \underbrace{\rho A \Delta x}_{M}
 \underbrace{\begin{bmatrix} 1 & 0 & 0 \\ 0 & 1 & 0 \\ 0 & 0 & 1 \end{bmatrix}}_{\ddot{u}}
 =
 \underbrace{\begin{bmatrix} -1 & 1 & 0 \\ 0 & -1 & 1 \\ 0 & 0 & -1 \end{bmatrix}}_B
 \underbrace{\begin{bmatrix} F_{01} \\ F_{12} \\ F_{23} \end{bmatrix}}_{F_s}
 +
 \underbrace{\begin{bmatrix} 0 \\ 0 \\ 0 \end{bmatrix}}_{F_{\text{ext}F}}
 \tag{1}$$

The state vector u consists of the mass deflections $(u_1, u_2, u_3)^T$, the vector of the spring force is $F_s = (F_{01}, F_{12}, F_{23})^T$, and the vector of the external force is $F_{\text{ext}F} = (F_{\text{ext}F1}, F_{\text{ext}F2}, F_{\text{ext}F3})^T$. It is noted that in Fig.1 no external forces are included, but for the derivation of a general solution of force- and stress tracking we take into account external forces. For the lumped model, effective masses m , stiffnesses k , damping parameters d and piezoelectric parameters c are to be computed following well-known procedures of structural mechanics. For that sake, mass density ρ , cross section A , Young's modulus $E = C_{11}$ as well as geometric and damping parameters of the bar are to be known. The length of one element is Δx , hence the mass of one element is $m = \rho A \Delta x$. The stiffness of the spring is $k = EA / \Delta x$. Depending on the mode of piezoelectric actuation, either by the transverse mode \tilde{e}_{31} or by the longitudinal mode \tilde{e}_{11} , this coefficient is calculated differently. The width is b and the height is h , hence the cross section is $A = bh$.

Equation (1) can be easily written as a matrix differential equation, which holds for a system with n masses

$$M\ddot{u} = BF_s + F_{\text{ext}F} \rightarrow \ddot{u} = M^{-1}(BF_s + F_{\text{ext}F}) \tag{2}$$

The structure of the mass matrix M , B and the vector $F_{\text{ext}F}$ can be easily generalized for a n -DOF system if eqs. (1) and (2) are compared. For the three-degree-of-freedom model, the constitutive relations for a piezoelectric material yield the internal force vector, by integrating the axial stress over the cross section. This reads



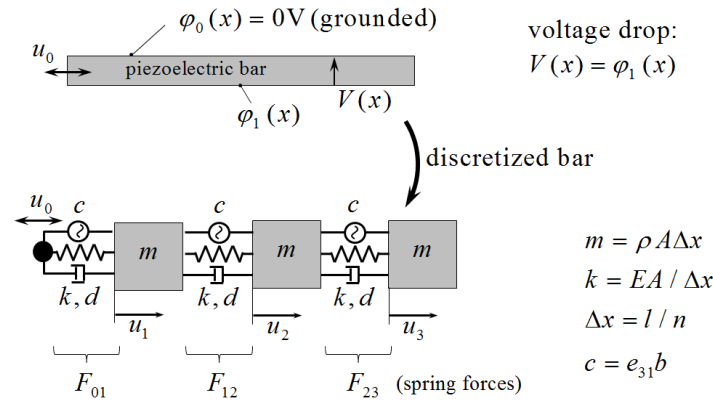


Fig. 1. Piezoelectric bar and the derived lumped element model with masses, stiffnesses and piezoelectric actuation.

$$\begin{aligned}
 F_{01} &= d(\dot{u}_1 - \dot{u}_0) + k(u_1 - u_0) + cV_1 \\
 F_{12} &= d(\dot{u}_2 - \dot{u}_1) + k(u_2 - u_1) + cV_2 \\
 F_{23} &= d(\dot{u}_3 - \dot{u}_2) + k(u_3 - u_2) + cV_3
 \end{aligned} \tag{3}$$

where u_0, \dot{u}_0 is the prescribed excitation (displacement and velocity) at the left end of the system. In matrix notation eq. (3) reads

$$F_s = D_1 \dot{u} + K_1 u + CV - (F_{ext u} + F_{ext \dot{u}}) \tag{4}$$

The piezoelectric matrix C is the identity matrix multiplied by the piezoelectric constant c , the matrices K_1, D_1 are associated with the stiffness and damping matrices and the state vector. Furthermore, the terms $F_{ext u} = (ku_0, 0, 0)^T$ and $F_{ext \dot{u}} = (d\dot{u}_0, 0, 0)^T$ reflect the force acting on mass 1 due to the boundary excitation and may not be accidentally mixed up with $F_{ext F}$, see eq. (1). It is noted that $F_{ext u} \neq 0, F_{ext \dot{u}} \neq 0$ holds for a support-excited system, while $F_{ext F} \neq 0$ holds for a force-excited system. The general, more familiar form of the governing equation in terms of the state vector is

$$M\ddot{u} = -D\dot{u} - Ku + F_a + F_{ext} \tag{5}$$

where the inertia-related term $M\ddot{u}$ is on the left hand side and the stiffness K and damping matrices D (with the associated state displacements and velocities), the vector of the piezoelectric actuation F_a and the vector F_{ext} are on the right-hand side. The goal is to combine eqs. (1)-(4) with eq. (5) to find a matrix differential equation for the internal force vector F_s : inserting eq. (4) into eq. (2), one finds the following relations by comparison with eq. (5)

$$\begin{aligned}
 K &= -BK_1 \\
 D &= -BD_1 \\
 F_{ext} &= -B(F_{ext x} + F_{ext \dot{x}}) + F_{ext F} \\
 F_a &= CBV
 \end{aligned} \tag{6}$$

Differentiating eq. (5) twice with respect to time, inserting higher time-derivatives of the state vector u from eq. (2) and taking into account eq. (6), one obtains the following differential equation for the piezoelectric actuation F_a :

$$\ddot{F}_a = B\ddot{F}_s + DM^{-1}(B\dot{F}_s + \dot{F}_{ext F}) + KM^{-1}(BF_s + F_{ext F}) + B(\ddot{F}_{ext u} + \ddot{F}_{ext \dot{u}}) \tag{7}$$

Considering the relation $F_a = BCV$ from eq. (6), one may easily solve for the actuation voltage V that is necessary for force control. The right hand side of eq. (7) shows that the actuation vector F_a depends on structural parameters (i.e. the stiffness matrix K , the damping matrix D and the mass matrix M and matrix B) as well as on the desired internal force vector F_s and the given external forces $F_{ext F}, F_{ext u}, F_{ext \dot{u}}$. Integration of eq. (7) twice with respect to time yields

$$F_a(t) = BF_s(t) + DM^{-1} \left(\int_{\bar{t}=0}^t BF_s(\bar{t}) + F_{ext F}(\bar{t}) d\bar{t} \right) + KM^{-1} \left(\iint_{\bar{t}=0}^t BF_s(\bar{t}) + F_{ext F}(\bar{t}) d\bar{t}^2 \right) + B[F_{ext u}(t) + F_{ext \dot{u}}(t)] + G_0 + G_1 t \tag{8}$$

Table 1. Geometry and material parameters for the piezoelectric transducer (PZT-5A).

Variable (unit)	Values	Description
ρ ($kg m^{-3}$)	7750	mass density
h (m)	$8.00 \cdot 10^{-4}$	height
b (m)	$5.00 \cdot 10^{-2}$	width
\tilde{e}_{31} ($As m^{-2}$)	-10.43	piezoelectric coefficient
$E = \tilde{C}_{11}$ ($N m^{-2}$)	$6.29 \cdot 10^{10}$	Young's modulus
M (kg)	10	end mass
l (m)	0.8	length



The integration constants G_0, G_1 can be determined as follows: considering the internal force F_s in eq. (4), one finds the following relation at $t = 0$

$$\begin{aligned} F_s(0) &= D_1 \dot{u}(0) + K_1 u(0) + CV(0) - [F_{ext\ u}(0) + F_{ext\ \dot{u}}(0)] \\ \rightarrow V(0) &= C^{-1} [F_s(0) - D_1 \dot{u}(0) - K_1 u(0) + F_{ext\ u}(0) + F_{ext\ \dot{u}}(0)] \end{aligned} \tag{9}$$

which can be easily solved for the initial voltage vector $V(0)$, or, equivalently, for the actuation vector $F_a(0) = CBV(0)$, see eq. (6). A second relation for the voltage is found by substituting the acceleration $\ddot{u}(t)$ from eq. (2) into the time derivative of eq. (4)

$$\begin{aligned} \dot{F}_s(0) &= D_1 \underbrace{M^{-1} [BF_s(0) + F_{ext\ F}(0)]}_{=\ddot{u}(0), \text{ see eq. (2)}} + K_1 \dot{u}(0) + C\dot{V}(0) - [\dot{F}_{ext\ u}(0) + \dot{F}_{ext\ \dot{u}}(0)] \\ \rightarrow \dot{V}(0) &= C^{-1} [\dot{F}_s(0) - D_1 M^{-1} [BF_s(0) + F_{ext\ F}(0)] - K_1 \dot{u}(0) + \dot{F}_{ext\ u}(0) + \dot{F}_{ext\ \dot{u}}(0)] \\ \rightarrow \dot{F}_a(0) &= CB\dot{V}(0) \end{aligned} \tag{10}$$

The right-hand sides of eqs. (9) and (10) are known, consequently also the initial voltage vector $V(0)$ and its time derivative $\dot{V}(0)$ from which the integration constants G_0, G_1 in eq. (8) are found. It is noted that from a practical point of view the choice of the prescribed internal force vector F_s is strongly limited because the actuation vector $F_a(t)$ depends on time integrals of $F_s, F_{ext\ u}, F_{ext\ \dot{u}}$ and $F_{ext\ F}$, but the excitation should not exceed certain bounds. Furthermore, the constant G_1 should be zero. If this is not the case, the necessary actuation vector becomes unbounded because it linearly increases with time, and, as a consequence, the state vector u may be unlimited, see eq. (2). This should be taken into account for practical realization.

3. Numerical Benchmark: Piezoelectric Bar with Prescribed Boundary Motion

For verification of the stress-control results (8)–(10), we consider a homogenous piezoelectric bar with end mass m_{end} (i.e. if we assume $n = 40$ equal lumped masses, the state vector of the right mass is u_{40} , which is associated with the mass $m + m_{end}$, c.f. Figs. 1 and 2a). The geometry and the material parameters can be found in Table 1. For the calculation of the effective values on beam level (for the PZT-5A material parameters \bar{e}_{31} and \bar{C}_{11}), the reader is referred to [25].

The support excitation at the left end is

$$u_0(t) = 0.0005 \left(\frac{e}{3} \right)^3 \left(\frac{t}{T} \right)^3 e^{-\frac{t}{T}} \tag{11}$$

where the variable e is Euler’s number. For clarity, eq. (11) is a special form of the impulse excitation $(t/T)^n e^{-(t/T)}$, which has a maximum value $n^n e^{-n}$ at $t = nT$. Inserting $n = 3$ and demanding a maximum peak value 0.5 mm, one finds the coefficient $(e/3)^3$ in eq. (11). The temporal distribution of the excitation $u_0(t)$ is depicted in Fig. 2c. Depending on the choice of the time constant T , one may tune the thickness of the (asymmetric) impulse-like excitation and its frequency content (see the single-sided frequency spectrum in Fig. 2d). A high value T means that only the lowest mode will be excited; low values for T mean that many eigenmodes may be excited by the support excitation. Here we consider three different cases of impulse-excitations in order to study low and high-frequency excitations:

- Quasi-static excitation $T = 1/250$ s (blue curves in Fig.2c and d, section 3.1)
- Dynamic excitation $T = 1/2500$ s (black curves in Fig.2c and d, section 3.2)
- High dynamic excitation $T = 1/12\ 500$ s (red curves in Fig.2c and d, section 3.3)

The idea behind these three types of actuation is to prove that the derived conditions for stress control hold for quasi-static excitations (hardly any dynamics or only the lowest mode) and also for high dynamic excitations. The bar is discretized as a damped lumped mass and spring system with $n = 40$ elements, from which the first three eigenfrequencies follow as

$$\begin{aligned} f_1 &= 87.5\text{Hz} \\ f_2 &= 1758.3\text{Hz} \\ f_3 &= 3512.7\text{Hz} \end{aligned} \tag{12}$$

The desired temporal and spatial distribution for the internal force vector is

$$F_s = G\rho A\ddot{u}_0(t) \tag{13}$$

where $G = [G_1, G_2, G_3, \dots, G_{40}]^T$ is the desired spatial distribution. For reasons of simplicity, the value of the element G_i is evaluated in the middle of each element, i.e. $G_9 \approx (g(x_9) + g(x_8))/2$ where $g(x)$ is the desired continuous spatial stress distribution, see Fig.2b (black)

$$g(x) = 1 \left[\left(\frac{x}{l} \right) - 3 \left(\frac{x}{l} \right)^2 + 3 \left(\frac{x}{l} \right)^3 - \left(\frac{x}{l} \right)^4 \right] \tag{14}$$

Inserting eq. (13) into eq. (2) and regarding that the external force vector vanishes $F_{ext\ F} = 0$, one finds the analytical solution for the displacement

$$u(t) = M^{-1} B G \rho A u_0(t) = \frac{1}{\Delta X} B G u_0(t) \tag{15}$$



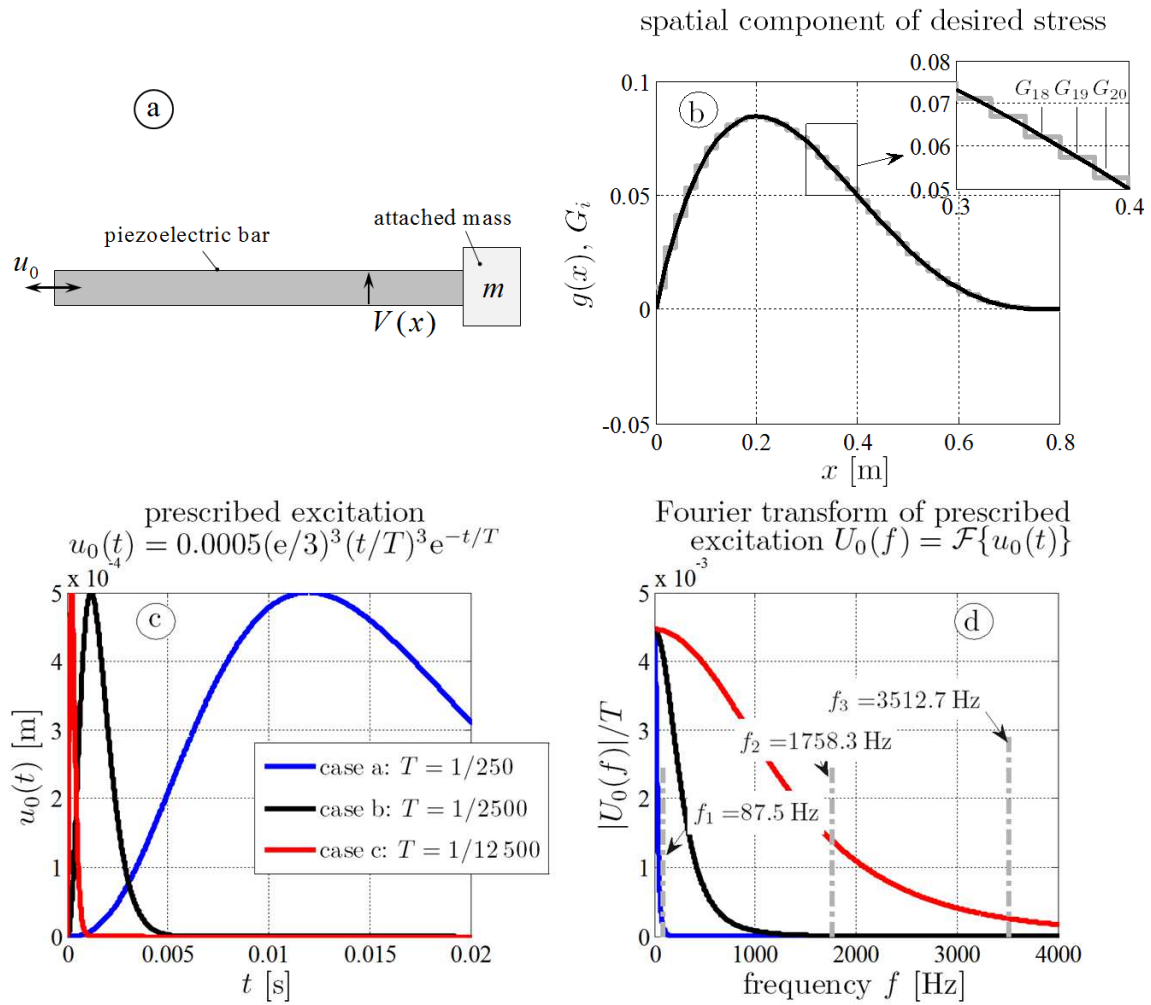


Fig. 2. (a) Piezoelectric transducer with end-mass M , (b) desired spatial distribution G_i of stress (zoom shows portions of the 18th, 19th and 20th element, see eq. (14)), (c) prescribed excitation $u_0(t)$ and (d) its frequency spectrum $U_0(f)/T$.

Comparing eq. (15) with a previous result of the authors (see eq. (35) in [22], the same problem is investigated, but as a continuous bar), the analytical solution for the displacement in case of stress control follows as $u(x,t) = g_x(x)u_0(t)$. One observes that the operation

$$\frac{1}{\Delta x}BG \approx g_x(x) \tag{16}$$

is approximately the differential quotient of the desired stress distribution (the matrix B from eq. (1) is applied to the matrix G in eq. (16)). Hence the theory for stress control for a discretized bar presented in this contribution converges to the solution for stress control of a continuous bar in [22]. It is noted that the matrix-based formulation presented here is advantageous, because it also takes into account damping, see eq. (8), which is not considered in the previous contribution of the authors in case of a continuous bar. Moreover, the matrix formulation is advantageous because the actuation vector $F_a(t)$ in eq. (7) depends on mass, stiffness and damping matrices, the desired stress distribution and the force vector. This allows for an easy implementation of realizing experiments. Additionally, it may serve as a starting for stress-control algorithm for other problems in structural mechanics (e.g. for plates, shells).

3.1 Quasi-static excitation – results for $T=1/250$ s

Figure 3 shows the results for the slowly-varying boundary excitation (i.e. $T = 1/250$ s, blue curves in Figs. 3c and d). Figures 3a and c show results (stress and displacement, exemplarily for locations close to left end ($x = l/20$), to the middle ($x = l/2$) and to the right end ($x = 4l/5$)) if the stress control method is active. Figures 3b and d show the results if stress-control is turned off (i.e. $F_a = 0$). Additionally, the maximal allowed tensile stress $\sigma_{\max}^{\text{PZT5A}} \approx 2.5 \times 10^7 \text{ Nm}^{-2}$ (green, see [28]) for a non-preloaded PZT ceramics is shown in Fig. 3c: this is approximately 10% of the maximum compressive pressure limit. Here both stress levels are below $\sigma_{\max}^{\text{PZT5A}}$: for the non-actuated bar, the stress is almost evenly distributed in the axial direction, oscillating at its first natural frequency $f_1 = 87.5 \text{ Hz}$ between $\pm 1 \times 10^7 \text{ Nm}^{-2}$. In contrary, the stress distribution is much smaller for the stress-controlled bar (i.e. $< 0.1\%$ of $\sigma_{\max}^{\text{PZT5A}}$). It is noted that although the stress differs several orders of magnitude, the displacements have the same order of magnitude for both the uncontrolled and the controlled configuration.



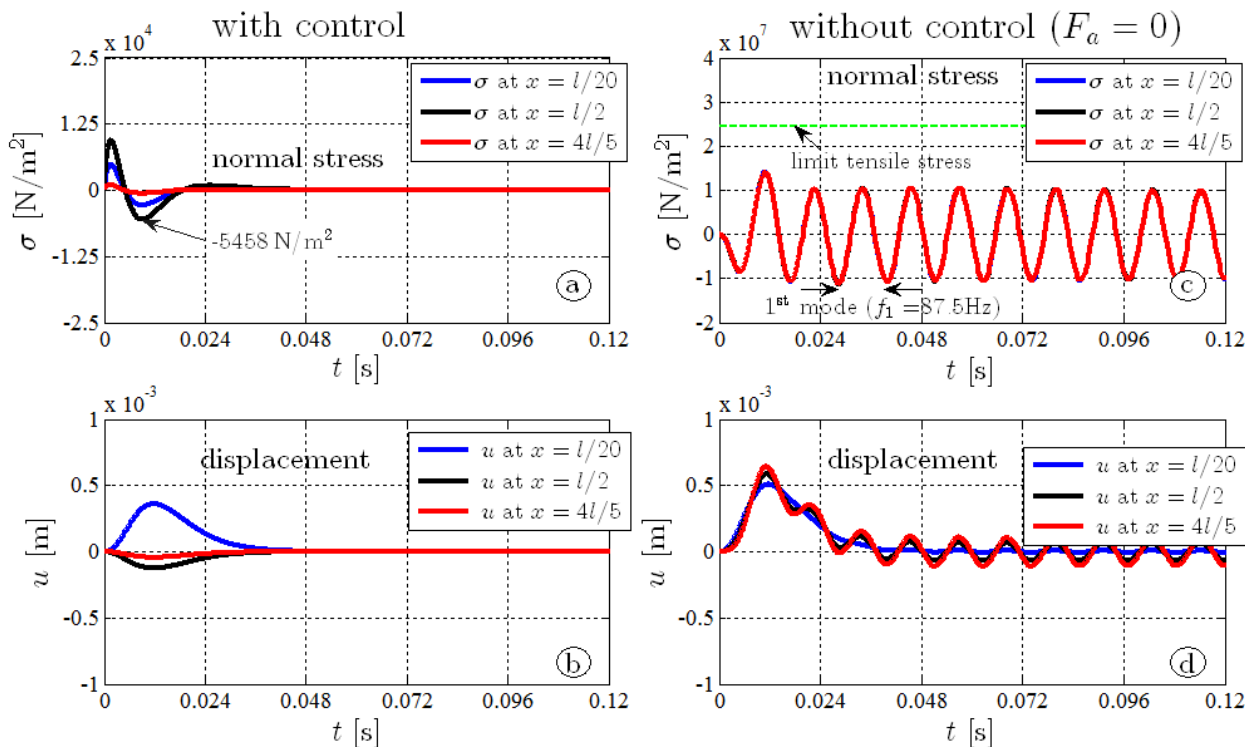


Fig. 3. Results for the internal stress σ and the displacement u with and without stress control for quasi-static excitation ($T = 1/250$ s).

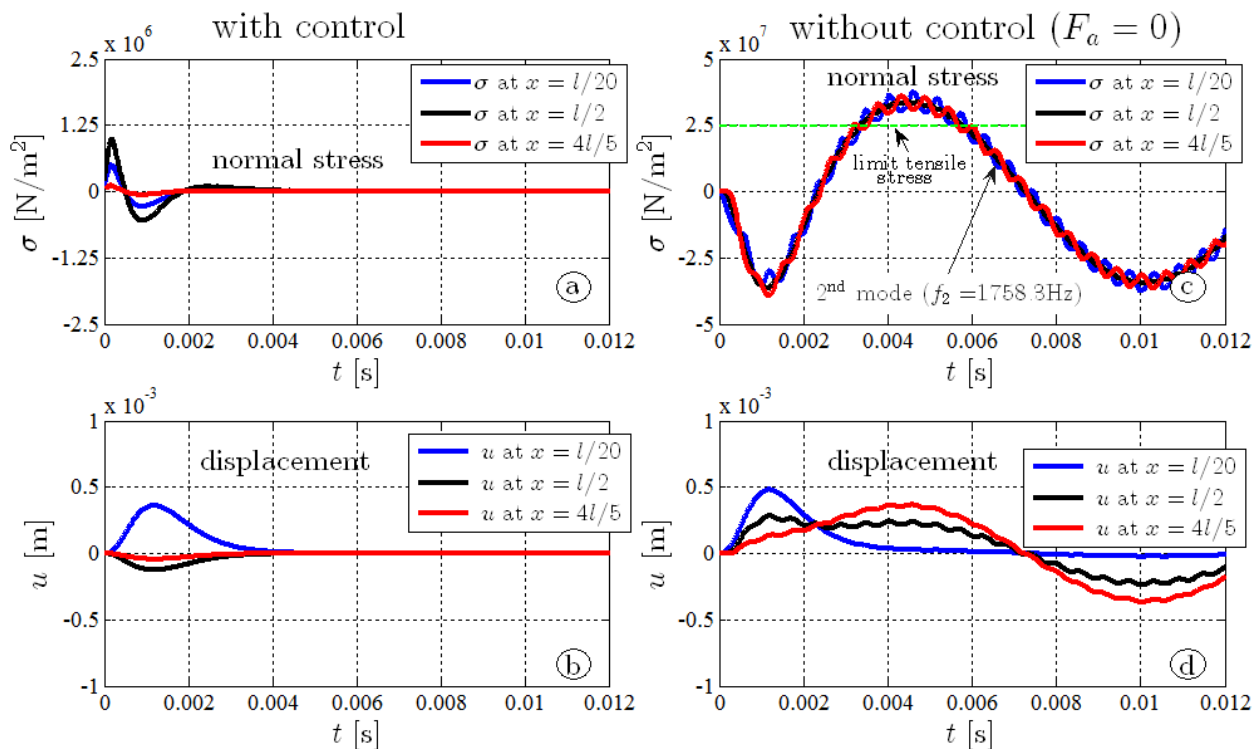


Fig. 4. Results for the internal stress σ and the displacement u with and without stress control for dynamic excitation ($T = 1/250$ s).

3.2 Dynamic excitation – results for $T=1/2500$ s

Figure 4 shows the results if the frequency content of the boundary excitation is increased (i.e. $T = 1/2500$ s, black curves in Figs. 4c and d). Now the first and also the second eigenmode are excited and the maximal axial stress is $3.75 \times 10^7 \text{ Nm}^{-2}$, which according to the datasheet provided by the manufacturer might cause a breakdown of the piezoelectric transducer. In case of stress-control (Fig. 4a), the maximum stress is only 5% of $\sigma_{\text{max}}^{\text{PZTSA}}$, which is far below the tensile stress limit.



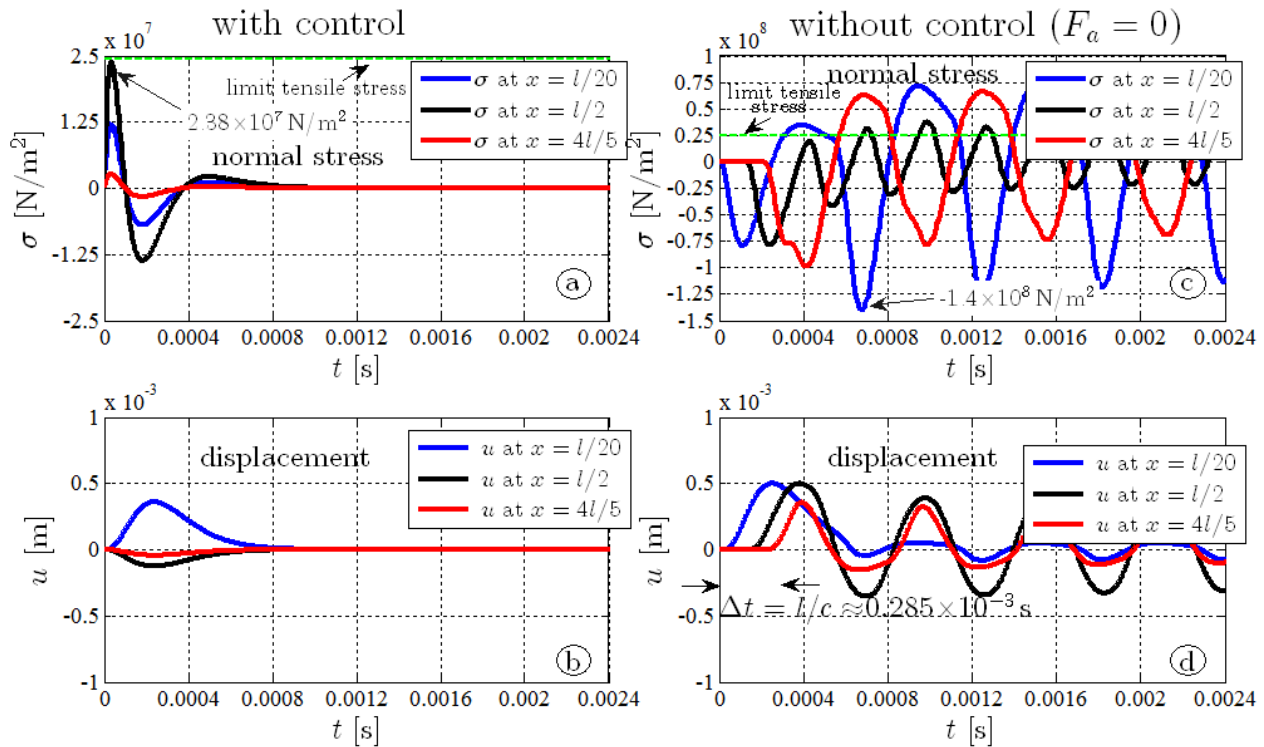


Fig. 5. Results for the internal stress σ and the displacement u with and without stress control for high dynamic excitation ($T = 1/12\,500$ s).

3.3 High dynamic excitation – results for $T=1/12\,500$ s

Figure 5 shows the results of a high-frequency peak of the boundary excitation (i.e. $T = 1/12500$ s, red curves in Figs. 5c and d). One observes the typical wave propagation phenomenon if stress-control is turned off: it takes about $\Delta t = 0.285 \times 10^{-3}$ s that the stress wave generated by the excitation reaches the attached mass, where it is partially reflected (note that $\Delta t = l/c$ holds with $c \approx \sqrt{E/\rho}$ as the wave velocity). Even in the case where the stress-control actuation is applied, the tensile stress is very close to the limit stress $\sigma_{\max}^{\text{PZTSA}}$ (at $x=l/4$, it will even exceed the limit stress, see Fig. 5b). This example shows that the stress cannot be controlled for arbitrarily high frequencies: this limitation for stress control is already pointed out by the author [23] for bending vibrations.

4. Experiment

4.1 Description of experimental setup and test procedure

For the verification of the above-described stress-control method, an experiment is realized (bottom Fig. 6 and Fig. 9b): it consists of a piezoelectric stack actuator (Piezocomposite – stack type actuator series PStVS with preload, PSt 1000/25/40 VS 35, piezosystem jena, see [26]) which on the one side is connected to a rigid support. It serves as an external actuation of a piezoelectric transducer (PICMA® stack multilayer piezo actuators, P-887.51, $7 \times 7 \times 18$ mm from PI physikinstrumente), see [27]. Loctite Hysol 9466 a&b serves as glue material, an electrically isolating two-component adhesive. Both the electrodes of the transducer and of the stack are linked to power amplifiers (AE Techron 7224) which amplify the control and actuation signals from the control unit by a factor of 20. In order to tune the first resonance frequency $f_1 = 5000$ Hz an attached end mass with $m_T = 0.0988$ kg (Table 2) is fixed to the end face of the transducer. The piezoelectric actuator serves as the disturbance source: the voltage signal of the disturbance V_A is a repeating sweep signal with a time period of 0.1s. During this period the frequency increases from 1000 Hz to 4900 Hz, which causes a temporal internal stress over the transducer cross section. In case of stress-control, this repeating sequence takes 1320s with a slowly increasing ramp (20s) at the beginning and a decreasing ramp (20s) at the end. By proper actuation of the piezoelectric transducer V_T (see eq. (8)), the goal is to reduce the internal stress level. Although this is theoretically possible for a system with exactly known system parameters, our main goal here is to show that the experiment does not suffer any damage if control is present (only if control is turned off). Due to the uncertainties of the parameters, open-loop forward methods may deviate from the ideal results that are calculated from computer-aided methods. Actuating the system with the same temporal excitation V_A , but without stress-control (i.e. the voltage of the piezoelectric transducers is $V_T=0$ V), the piezoelectric transducer is expected to fail if the maximum tensile damage force F_{damage} is exceeded for a certain amount of time or cycles. According to manufacturer's datasheet specification the damage value cannot be specified exactly, it is estimated to 10 % of the blocking force $F_{\text{blocking}}=1750$ N, see [27].

Table 2. Estimated parameters of the experiment.

Parameter	Value	Unit
m_A	0.163	kg
m_T	0.0988	kg
k_A	$585 \cdot 10^6$	N/m
k_T	$130 \cdot 10^6$	N/m
d_A	300	Ns/m
d_T	400	Ns/m
c_T	25	N/V
c_A	16.25	N/V



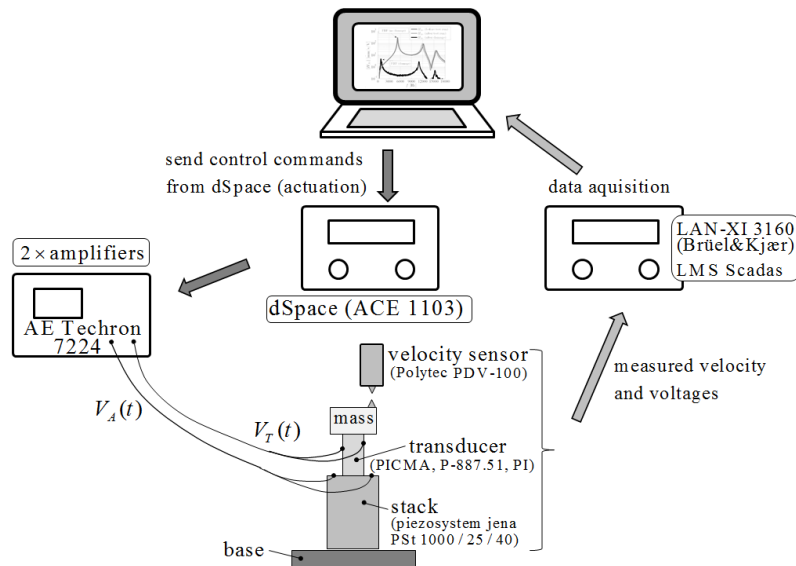


Fig. 6. Experimental setup, control and measurement devices for the realization of stress control.

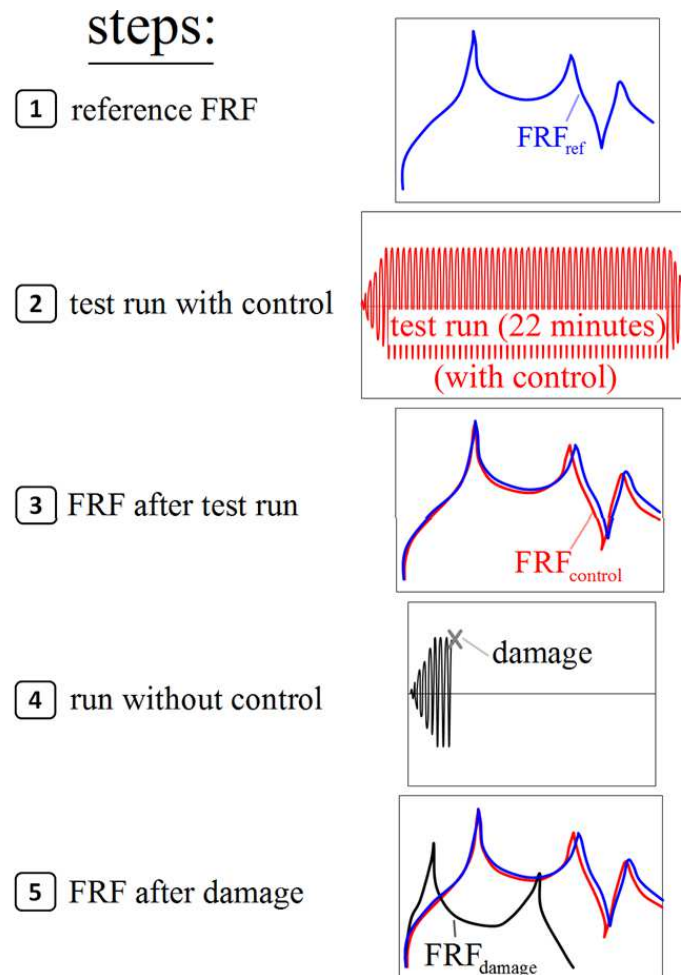


Fig. 7. Five steps of the test procedure: the original FRF is measured (step 1) before the stress-controlled run (22minutes, step 2). After measuring the FRF again (step 3), only the stack actuator is actuated (i.e. $V_A(t) \neq 0$ V, transducer voltage $V_T(t) = 0$ V, step 4, see eq. (8)). The final FRF should verify the damage (significant change of FRF, step 5).

The whole system is modeled as a simple 2DOF system, the estimated parameters are shown in Table 2. The masses of the 2DOF system are m_A and m_T , the stiffnesses k_A and k_T , the damping coefficients d_A and d_T , and the piezoelectric coupling coefficients c_A and c_T . It is worthy to note that these values do not really reflect those available from the datasheet, see [26, 27]. First the transducers mass m_T contains half of the transducers mass and of the attached mass. In general these values are varied such that the frequency responses of the 2DOF system (with actuator and transducer voltage as inputs and velocity as output) are in good agreement with the measured responses from the experiment. In a last step the damping values d_A and d_T are varied such that the resonance peaks match.



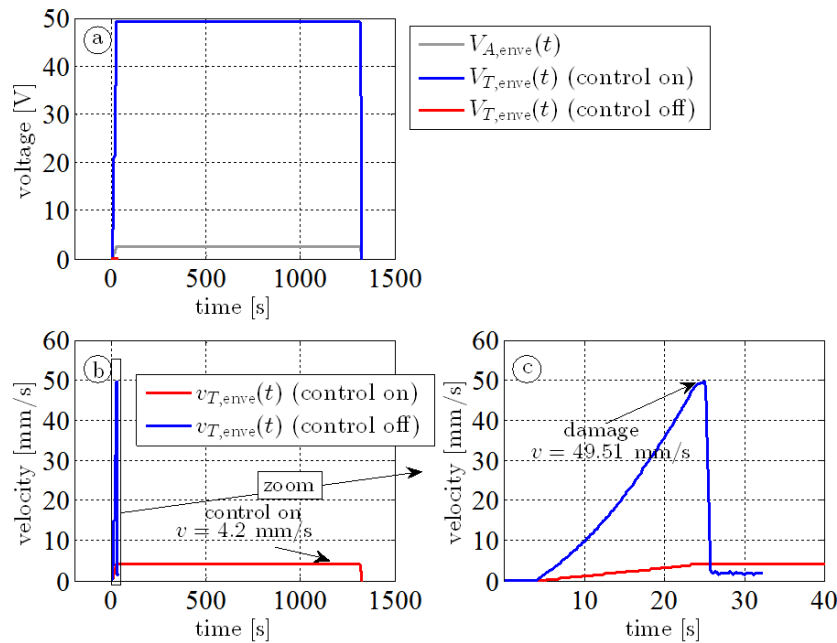


Fig. 8. Envelope curves: (a) voltage and control actuation, (b) velocity of attached mass, (c) velocity with zoom.

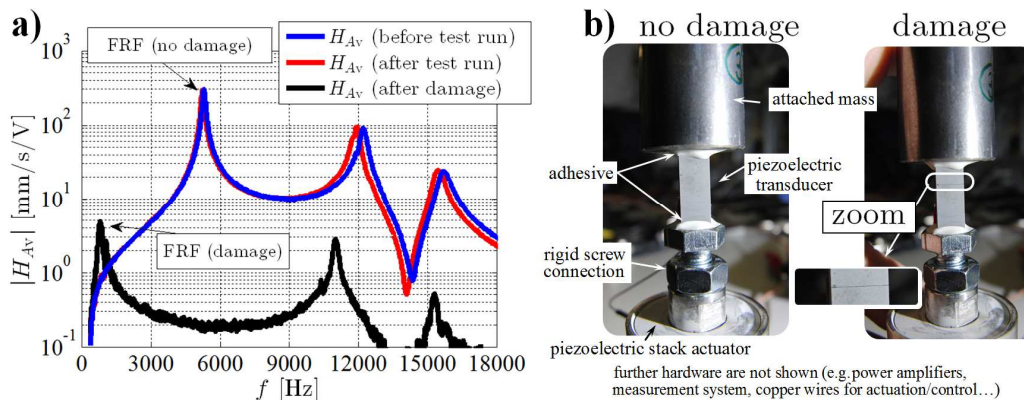


Fig. 9. (a) Frequency response functions (before controlled test run – blue, after controlled test run – red, after damage – black), (b) Undamaged and damaged experiment.

In order to verify our stress control theory experimentally, the velocity of the attached mass is measured (device Polytec PDV-100). The transducer force can be calculated from the velocity by taking its time derivative and multiplication with m_T . The control and the actuation signal entering the power amplifiers (AE Techtron 7224) are generated by dSpace ACE 1103 (hardware) and dSpace Control Desk (software). The real time C-code for this rapid prototyping control soft/hardware is generated from a MATLAB/Simulink model, where the stress-control equations have been implemented by basic Simulink blocks. For the frequency response function measurements (steps 1, 3 and 5 in Fig. 7) LAN-XI type 3160 from Brüel&Kjær is used for data acquisition (the sampling frequency is 32,768 Hz). SCADAS Mobile and SCADAS recorder are used for capturing the dynamic signals for the controlled and uncontrolled test runs (steps 2 and 4 in Fig. 7) with a 204.8 kHz rate for the data channels.

A critical point is the question what does mechanical damage, failure or breakdown exactly mean? Here damage means a mechanical damage caused by an excessive stress level. In contrary, the change of polarization or modified piezoelectric parameters is not considered as damage. Our strategy is to exceed the maximum tensile force in case of “no-stress-control”, while staying below the critical level in case of “stress-control”. Hence in order to introduce an objective criterion and an indicator for this occurrence, this involves a substantial loss of stiffness, i.e. the eigenfrequency will decrease.

Figure 7 shows five steps of the test procedure: First, the frequency response function (FRF) $H_{Av}(\omega) = v_T(\omega)/V_A(\omega)$ is measured (step 1), which is denoted as reference FRF. The input signal is the actuation voltage $V_A(\omega)$, the output is the velocity of the mass $v_T(\omega)$. Then the system is driven in control-mode (step 2) for 1320s (≈ 22 min), i.e. the stress-control signal is present, see eq. (8). In this phase the setup undergoes approximately 4×10^6 stress cycles as a consequence of the repeating sweep actuation. The FRF is measured again (step 3), which should be identical to the reference FRF measured in step 1. Then the destruction phase begins (step 4) and the piezoelectric transducer signal is turned off: $V_A \neq 0, V_T = 0$. The damage force is between 10% of the blocking force $F_{damage} \approx 0.1 \times F_{blocking} \approx 175$ N. This step is aborted if a breakdown of the system is noticed (e.g. by audible indication). Finally, the FRF is measured (step 5), which then provides an objective evidence for damage.

4.2 Results

Figure 8 shows the envelopes of the results ($V_{A,ENVE}(t)$, $V_{T,ENVE}(t)$, $v_{T,ENVE}(t)$) from the experiment. The actuation voltage reads $V_A(t) = V_{A,ENVE}(t) \cdot s(t)$, where $s(t)$ is the sweep signal with unit amplitude (except at the beginning and at the end) whose frequency linearly increases and decreases from 1000 Hz to 4900 Hz during the period $\Delta t = 0.1$ s. This also holds for the transducer control signal $V_T(t)$ and $v_{T,ENVE}(t)$ in a similar fashion.



In the beginning, the (envelope of the) actuation voltage $V_{A,ENVE}(t)$ increases linearly from 0 V to 49.2 V over 20 s (between 4 s and 24 s, Fig. 8a). If the stress-control mode is active, the transducer voltage increases from 0 V to 2.46 V, causing a maximum peak 4.2 mm/s (Fig. 8b–red) for the velocity of the mass. This remains almost constant during the 22min test run. For the uncontrolled configuration, one observes that the maximum actuation voltage is reached at $t = 24$ s, which is followed by an immediate decline and the test run is aborted (Figs. 8b and c–blue): the maximum velocity $v_{T,ENVE}(t) = 49.5$ mm/s means a transducer force $F_T = 150$ N $\approx F_{damage}$. The FRFs in Fig. 9a show that the frequency curve after the destruction phase has a completely different shape as those measured at the beginning (blue) and immediately after the controlled test run (light blue): One observes a notable shift of the first eigenfrequency from 5300 Hz to 818 Hz. Furthermore it should be noted that the measured FRF of the broken setup shows a high noise level in the FRF, which has not been observed for the previous ones (compare the black curve to the blue and red one in Fig. 9a). Further signs of damage are shown in Fig. 9b where one observes a crack line on the surface of the transducer.

5. Conclusion

In this contribution, stress-tracking is investigated for a lumped-element model of a piezoelectric transducer. The equations of motion are set up in matrix-notation first. After introducing the vector for the internal forces, which consists of a mechanical part (i.e. spring force with damping) and an electrical part (i.e. piezoelectric eigenstrain), the differential equations are transformed into second order differential equations with the internal force as the new state vector. Solving these matrix equations for the piezoelectric actuation, which are directly related to the applied voltage distribution, one finds a relation for the necessary actuation source in order to perform stress control as a function of the geometry, the material parameters, the external forces and the excitations. The stress-control theory is verified by means of a support-excited piezoelectric bar. Finally an experimental setup is realized: the configuration is exposed to a boundary excitation (i.e. a sweep signal with frequency content between 1000–4900 Hz). While the force-controlled remains undamaged after a 22 minutes test run, the uncontrolled configuration gets damaged after several load cycles.

Author Contributions

J. Schoeftner sets up the theory of stress control for the MDOF system, carried out the computations and is responsible for the implementation of the stress control C-code (MATLAB/Simulink, dSpace). The underlying stress control theory for three-dimensional continua is based on the mathematical formulation of H. Irschik, who also had the idea for the 2DOF experiment. A. Brandl is responsible for the design of the experimental setup, the hardware and the measurement devices.

Conflict of Interest

The authors declared no potential conflicts of interest with respect to the research, authorship and publication of this article.

Funding

The authors received no financial support for the research, authorship, and publication of this article.

References

- [1] Yang, J., *Analysis of Piezoelectric Devices*, World Scientific, Hackensack, NJ, 2006.
- [2] Preumont, A., *Mechatronics: Dynamics of Electromechanical and Piezoelectric Systems*, Springer, 2006.
- [3] Safari, A., Akdogan, E.K. (Eds.), *Piezoelectric and Acoustic Materials for Transducer Applications*, Springer, 2008.
- [4] Moheimani, S.O.R., Fleming, A.J., *Piezoelectric Transducers for Vibration Control and Damping*, Springer, London, 2006.
- [5] Irschik, H., A review on static and dynamic shape control of structures by piezoelectric actuation, *Engineering Structures*, 24, 2002, 5–11.
- [6] Irschik, H., Krommer, M., Nader, M., Schöftner, J., Zehetner, C., Active and Passive Shape Control of Structures, *Proceedings 5th European Conference on Structural Control (EACS 2012)*, E. Del Grosso, P. Basso. (Eds.), Genua, Italy 2012, Paper No. 146, 8 pages, 2012.
- [7] Irschik, H., Krommer, M., A Review on Static and Dynamic Shape Control of Structures: The Period 2002–2012, *Proceedings Vienna Congress on Recent Advances in Earthquake Engineering and Structural Dynamics 2013 (VEESD 2013)*, C. Adam, R. Heuer, W. Lenhardt, C. Schranz (Eds.), Vienna, Austria 2013, Paper No. 581, 2013.
- [8] Irschik, H., Krommer, M., Zehetner, Ch., Displacement tracking of pre-deformed smart structures, *Smart Structures and Systems*, 18, 2016, 139–154.
- [9] Austin, F., Rossi, M.J., Van Nostrand, W., Knowles, G., Static shape control of adaptive wings, *AIAA Journal*, 32, 1994, 1895–1901.
- [10] Agrawal, B.N., Treanor, K.E., Shape control of a beam using piezoelectric actuators, *Smart Materials and Structures*, 8, 1999, 729–740.
- [11] Schoeftner, J., Irschik, H., Passive damping and exact annihilation of vibrations of beams using shaped piezoelectric layers and tuned inductive networks, *Smart Materials and Structures*, 18, 2009, 125008 (9pp).
- [12] Schoeftner, J., Irschik, H., Passive shape control of force-induced harmonic lateral vibrations for laminated piezoelectric Bernoulli–Euler beams—theory and practical relevance, *Smart Structures and Systems*, 7, 2011, 417–432.
- [13] Schoeftner, J., Buchberger, G., Brandl, A., Irschik, H., Theoretical prediction and experimental verification of shape control of beams with piezoelectric patches and resistive circuits, *Composite Structures*, 133, 2015, 746–755.
- [14] Schoeftner, J., Irschik, H., Buchberger, G., Static and dynamic shape control of slender beams by piezoelectric actuation and resistive electrodes, *Composite Structures*, 111, 2014, 66–74.
- [15] Schoeftner, J., Buchberger, G., Active shape control of a cantilever by resistively interconnected piezoelectric patches, *Smart Structures and Systems*, 12, 2013, 501–521.
- [16] Giorgio, I., Culla, A., Del Vescovo, D., Multimode vibration control using several piezoelectric transducers shunted with a multiterminal network, *Archive of Applied Mechanics*, 79, 2009, 859–879.
- [17] Lossouarn, B., Deü, J. F., Aucejo, M., Multimodal vibration damping of a beam with a periodic array of piezoelectric patches connected to a passive electrical network, *Smart Materials and Structures*, 24(11), 2015, 115037.
- [18] Rosi, G., Pouget, J., dell'Isola, F., Control of sound radiation and transmission by a piezoelectric plate with an optimized resistive electrode, *European Journal of Mechanics-A/Solids*, 29(5), 2010, 859–870.
- [19] Trindade, M.A., Maio, C.E.B. Multimodal passive vibration control of sandwich beams with shunted shear piezoelectric materials, *Smart Materials and Structures*, 17(5), 2008, 055015 (10 pages).
- [20] Benjeddou, A., Ranger, J. A., Use of shunted shear-mode piezoceramics for structural vibration passive damping, *Computers and Structures*, 84, 2006, 1415–1425.
- [21] Lediaev, L., *Finite element modeling of piezoelectric bimorphs with conductive polymer electrodes*, doctoral thesis Montana State University, Bozeman, Montana, 2010.
- [22] Suresh, S., *Fatigue of Materials*, 2nd Edition, Cambridge University Press, 1998.
- [23] Schijve, J., *Fatigue of Structures and Materials*, 2nd Edition, Springer, 2009.
- [24] Weisshaar, T., *Aerospace Structures – an Introduction to Fundamental Problems*, West Lafayette, In: Purdue University, 2011, (<https://engineering.purdue.edu/AAECourses/aae352/2013/AAE%20352%20Course%20Text%20Weisshaar%202011.pdf>).



- [25] Irschik, H., Generation of transient desired displacement or stress fields in force loaded solids and structures by smart actuation, in: *Proc. XXXV Summer School Advanced Problems in Mechanics (APM2007)*, Saint-Petersburg, Russia, 2007.
- [26] Irschik, H., Krommer, M., Gusenbauer, M., Tracking of Stresses: A Further Step towards Ageless Structures. in: H. Irschik, M. Krommer, K. Watanabe, T. Furukawa (Eds.), *Proc. 1st Joint Japan-Austria Workshop Mechanics and Model Based Control of Smart Materials and Structures*, September, 2008, Linz, Austria, Springer Wien New York, 77–84, 2009.
- [27] Irschik, H., Gusenbauer, M., Pichler, U., Dynamic stress compensation by smart actuation, in: R.C. Smith (Ed.), *Proceedings of SPIE on Smart Structures and Materials 2004: Modeling, Signal Processing, and Control*, San Diego, CA, 2004, SPIE vol. 5383, Paper No. 386, 2004.
- [28] Schoeftner, J., Irschik, H., Stress tracking of piezoelectric bars by eigenstrain actuation, *Journal of Sound and Vibration*, 383, 2016, 35–45.
- [29] Schoeftner, J., Bending moment tracking and the reduction of the axial stress in vibrating beams by piezoelectric actuation, *Acta Mechanica*, 228, 2017, 3827–3838.
- [30] Schoeftner, J., Brandl, A., Irschik, H., Control of stress and damage in structures by piezoelectric actuation: 1D theory and monofrequent experimental validation, *Structural Control and Health Monitoring*, 26(5), 2019, e2338 (14pp).
- [31] Schoeftner, J., Irschik, H., A comparative study of smart passive piezoelectric structures interacting with electric networks: Timoshenko beam theory versus finite element plane stress calculations, *Smart Materials and Structures*, 20, 2011, 025007 (13pp).
- [32] Website of the manufacturer of the piezoelectric stack: https://www.piezosystem.com/fileadmin/Piezocomposite/Datenblaetter/Aktoren/en/Stapel/VS/PSt_1000_VS_35_ds_Rev00_2017_01_09.pdf (February 26th, 2018).
- [33] Website of the manufacturer of the piezoelectric transducer: https://www.physikinstrumente.de/fileadmin/user_upload/physik_instrumente/files/datasheets/P-882-Datenblatt.pdf (February 26th, 2018).
- [34] Dent, A.C.E., Bowen, C.R., Stevens, R., Cain, M.G., Stewart, M., Tensile Strength of Active Fibre Composites Prediction and Measurement, *Ferroelectrics*, 368, 2008, 209–215.

ORCID iD

Juergen Schoeftner  <https://orcid.org/0000-0003-2990-4102>

Hans Irschik  <https://orcid.org/0000-0001-6593-243X>



© 2021 Shahid Chamran University of Ahvaz, Ahvaz, Iran. This article is an open access article distributed under the terms and conditions of the Creative Commons Attribution-NonCommercial 4.0 International (CC BY-NC 4.0 license) (<http://creativecommons.org/licenses/by-nc/4.0/>).

How to cite this article: Schoeftner J., Brandl A., Irschik H. Stress Control of a Piezoelectric Lumped-element Model – Theoretical Investigation and Experimental Realization, *J. Appl. Comput. Mech.*, 7(SI), 2021, 1110-1120.
<https://doi.org/10.22055/JACM.2020.33327.2203>

